Research Article Vol. 12, No. 9 / 1 Sep 2022 / Optical Materials Express 3638
Optical Materials EXPRESS

Tunable plasmonics with Au nanoparticles coupled to thin film vanadium dioxide

STEPHEN CUNNINGHAM AND A. LOUISE BRADLEY*

School of Physics and AMBER, Trinity College Dublin, College Green, Dublin 2, Ireland
*bradlel@tcd.ie

Abstract: The development of active devices featuring dynamic tunable plasmonic resonances is vital for wide implementation in many optoelectronic devices. By coupling plasmonic nanoparticles to an underlying thin film of phase change material vanadium dioxide (VO_2), dynamic tuning of the plasmon resonance can be achieved within the visible and near IR spectral regions. It is shown through selection of single nanoparticle or dimer structures, the plasmon resonances can be tuned over a large spectral range, the scattering cross-section can be increased, and the E-field enhancement and spatial profile can be controlled *via* the VO_2 phase transition. Hybrid Au nanocuboid–VO_2 structures exhibit larger reversible wavelength shifts than rounded nanoparticles, such as rods and discs, of similar dimensions. A plasmon resonance shift of over 600 nm is observed in the near-IR after the semiconducting to metallic VO_2 phase transition. The largest increases in the scattering cross-section are achieved with a VO_2 thin film thickness of 30–50 nm. Disc, rod, bowtie and cuboid dimers show larger increases of the scattering cross-section at lower wavelengths, even extending into the visible spectral range. On VO_2 phase transition the bowtie dimers can provide an increase in the scattering cross-section of over 70% and 3.6-fold increase in the E-field intensity within the dimer gap. Additionally, the near-field enhancement spreads over the entire height of the dimer gap, and in particular, there is a large enhancement at the surface of the dimers. The increased scattering cross-section and modification of the spatial profile of the E-field enhancement provides mechanisms for tunable metasurfaces.

1. Introduction

Over the past two decades much research has focused on the use of plasmonic nanostructures and metamaterials for the precise control of electromagnetic radiation. Utilizing plasmon resonances arising from noble metal nanoparticles is extremely attractive due to the vast range of applications in the field of nanophotonics. The optical response of such structures is highly dependent on the size, shape and material composition, factors generally set during the fabrication process. Many previous studies have focused on broadening the spectral range, for applications in perfect absorption or invisibility cloaking [1] or narrowing the spectral response for the development of sensors with increased sensitivity [2]. Despite the promise of plasmonics and metamaterials for miniaturization and on-chip integration, for many optoelectronic applications, such as optical modulators, switches, filter and polarisers, the inability to tune the optical response after fabrication becomes a limiting factor. To overcome this barrier, we consider plasmonic systems in which the optical properties can be dynamically tuned *via* an external stimulus. Our proposed hybrid system of tunable plasmonic elements consists of noble metal nanostructures coupled to an underlying layer of thin film vanadium dioxide (VO_2) which is a phase change material (PCM).

VO_2 is an attractive material option due to its highly reversible phase transition at a critical temperature of 68°C [3], a temperature significantly closer to room temperature than other rival

#462574 https://doi.org/10.1364/OME.462574
Journal © 2022 Received 2 May 2022; revised 8 Jul 2022; accepted 20 Jul 2022; published 16 Aug 2022

Corrected 22 August 2022

Optical Materials EXPRESS

PCMs such as GeSbTe (GST) [4] or AgInSbTe (AIST) [5]. At the critical temperature VO_2 transitions from a low temperature semiconducting monoclinic (M1) phase to a high temperature metallic rutile (R) phase. In addition to thermal actuation [3] of the VO_2 phase change, the transition can be triggered electrically [6] and optically [7] again at lower thresholds than rival PCMs and high switching speeds making VO_2 highly advantageous for dynamic tuning applications. The electronic and structural change in VO_2 is accompanied by a substantial change in the refractive index. While much previous VO_2 research has focused on the larger changes in the dielectric function in the NIR and IR spectral region above 900 nm [8], the changes seen at lower wavelengths can still have a significant impact on the optical response of resonant structures. Modulations of reflectance and absorbance of up to 35% in the visible to near infrared have been demonstrated for flat unpatterned resonant structures [9]. Colour tuning and a reflectance modulation of > 25% at 550 has been reported for thin film VO_2 in a multilayer stack configuration [10].

There have been relatively few reports considering tuning localised surface plasmon resonances (LSPRs) at wavelengths below 1 μm using the semiconductor to metal transition in VO_2. In Lei *et al.* it was shown that the plasmon resonance of a 100 nm diameter Au nanosphere blueshifts by 30 nm from 630 nm to 600 nm when the underlying VO_2 layer is heated from 30 °C to 90°C [11]. Tuning after deposition of VO_2 thin films on Au NPs has also been considered with larger blue-shifts reported [12], however the regions of high field enhancement cannot be easily accessed. The LSPR wavelength of a layer of Ag nanoparticles was shown to reversibly blueshift by 50 nm (with λ_{res} moving from 650 nm to 600 nm) and 252 nm (with λ_{res} moving from 956 nm to 704 nm) [13]. The addition of a TiO_2 dielectric layer of 30 nm thickness, not only causes a red-shift of the LSPR peak but increases the LSPR absorption and makes the tailoring of the plasmon resonance more pronounced [14]. Further, it increases the tuning range of the LSPR, doubled to approximately 100 nm from ~650 nm to 750 nm for 2 nm diameter Ag nanoparticles [15]. More recently, it was shown that tuning the plasmon resonance of a Ag nanodisc *via* the transition of VO_2 from the semiconducting to metallic phase could compensate for thermal emission quenching at elevated temperatures [16]. Other researchers have considered tunable Mie resonances of VO_2 nanoantennas [17] or through the use of Sb_2S_3 antenna arrays [18].

Herein, we explore the tunability of the LSPR, scattering cross-section and modification of the spatial E-field for a range of single Au nanoparticles and dimers. It will be shown that large spectral tuning can be achieved and accompanied by increases in the scattering cross section. Furthermore, dimer structures offer exciting possibilities for enhancing the E-field within the gap and at the surface of the dimer. Additionally, we address the absence of reports on the impact of VO_2 thin film thickness on the plasmonic response of single nanoparticle structures. The nanoparticles examined in this work can be easily fabricated for experimentation through standard electron beam lithographic methods and metal evaporation making these hybrid nanostructures well suited for nanophotonic applications. The VO_2 dielectric function used in numerical simulations was taken from a 30 nm VO_2 sample on a c-Al_2O_3 substrate fabricated by pulsed laser deposition and was measured using spectroscopic ellipsometry and is shown in Fig. 1(a). For each anisotropic structure a scattering cross section was calculated along the long axis (longitudinal plasmon) and the short axis (transverse plasmon). A schematic of the VO_2 – plasmonic nanoparticle structure is shown in Fig. 1 (b) with the propagation direction of the incident light, the direction of the E-field and H-field oscillation shown in red, blue and green, respectively. For all numerical simulations Al_2O_3 was used as the substrate material due to the lattice match with VO_2 which allows for improved VO_2 film crystallinity. The numerical simulations were done using the finite difference time domain (FDTD) solver of the commercial software Lumerical. Perfectly matched layers were set as the boundary condition with a plane wave total-field scattered-field (TFSF) excitation normally incident on the structure. A mesh size

Optical Materials EXPRESS

of 2.5 nm in the x, y and z direction for the plasmonic Au particles. For VO_2 a mesh size of 0.5 nm was used in the z-direction.

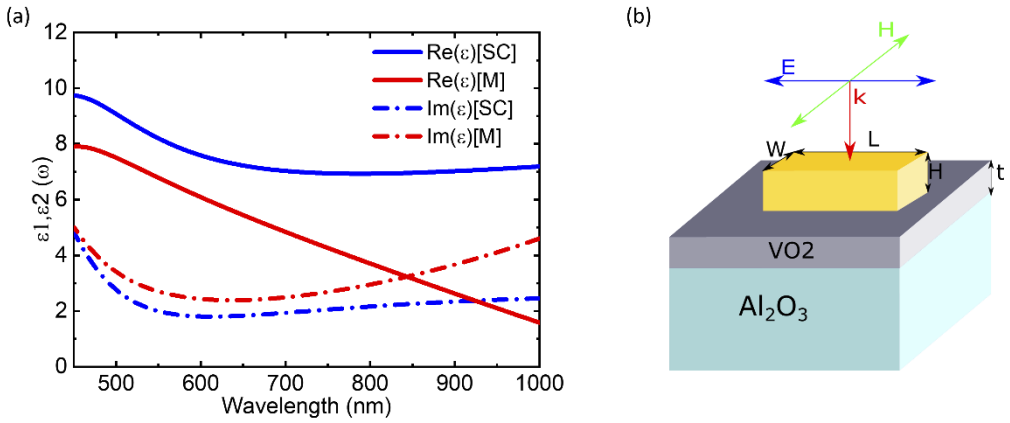

Fig. 1. (a) Real and imaginary parts of the dielectric function of VO_2 in the semiconducting (SC) and metallic (M) phases. (b) Schematic of a Nanoparticle-VO_2 structure with an Au nanocuboid of length L, width W, height H and VO_2 thickness t. The direction of propagation of light in the simulation is given by red arrow (k) with the blue and green arrows representing oscillation of the E-field and H-field, respectively, for a longitudinally polarized light source.

2. Results and discussion

Firstly, several single nanoparticle geometries were selected for investigation. Rod and cuboid shaped nanoparticles were selected due to their anisotropic shape which allow for the excitation of multiple plasmonic features. The plasmonic response of these particles for VO_2 in both phases was compared to the response seen for nanodiscs which, due to rotational symmetry, has degenerate resonances at each polarization angle.

Figure 2(a) shows the impact of nanoparticle height on the longitudinal (labelled P0) plasmon scattering spectra of a Au nanocuboid (Length = 180 nm, Width = 90 nm, Height = 10, 20, 40, 60, 80, 100 nm) on a 10 nm VO_2 thin film, in both the semiconducting and metallic phase. Increasing the nanoparticle height blueshifts the plasmonic response for both VO_2 phases, with the larger blueshift occurring for semiconducting phase VO_2. This results in a smaller shift in peak wavelength between the two VO_2 phases, however this smaller shift is accompanied by an increase in the magnitude of the scattering cross section, σ, as well as a larger positive Δσ ($\sigma_M - \sigma_{SC}$) in the visible spectral region. Increasing nanoparticle height also results in the emergence of a plasmonic feature at 600 nm corresponding to oscillation perpendicular to the VO_2 plane. There is no change in the position of this feature after the phase transition due to the significantly smaller difference in VO_2 optical constants in this wavelength range. The peak wavelength shift is larger for the lower nanocuboid heights as the resonances occur at higher wavelengths, where a larger change in the dielectric permittivity occurs after the VO_2 phase transition. In the range of interest below 1500 nm, the plasmon peak wavelength shifts by 285 nm for the 20 nm high nanocuboid. In Fig. 2(b) the impact of the nanoparticle height on the transverse (labelled P90) plasmonic response of the Au nanocuboid can be seen. As with the longitudinal plasmon response, there is a spectral blueshift with increasing height, and a narrowing of the plasmon resonance peak. In this case, once the structure height is greater than 40 nm there is no further impact on the scattering spectrum. While there is no region of increased scattering in the visible spectral range, the semiconducting to metallic phase transition can modulate the

Optical Materials EXPRESS

scattering cross-section by approximately a factor of 3. In Fig. 2(c) the impact of increasing width of the Au nanocuboid on the longitudinal resonance feature is examined. The nanocuboid height is fixed at 40 nm with the width varied from 30 nm to 180 nm. An increased width results in a blue-shifted longitudinal plasmon response with an increasing scattering cross-section. In the case of the transverse plasmon (Fig. 2(d)) the resonance is shifted to longer wavelengths. In both cases the plasmon peak blue shifts by up to 200 nm with the phase transition of VO_2.

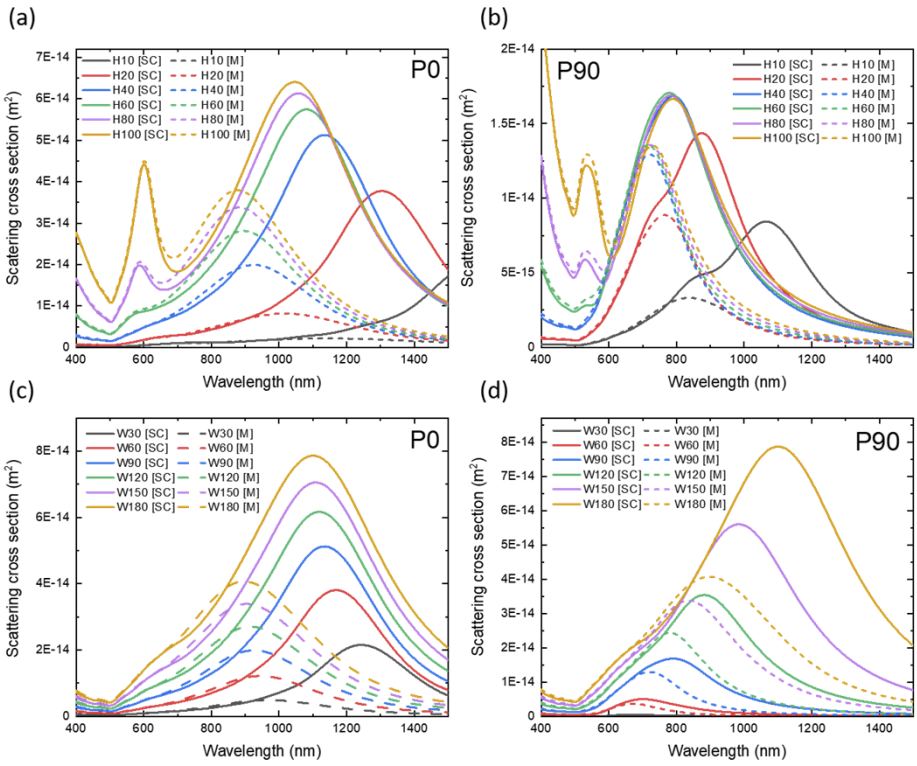

Fig. 2. Au Nanocuboid (Length = 180 nm, Width = 90 nm, Height = 10, 20, 40, 60, 80, 100 nm) for VO_2 (10 nm) in semiconducting phase (solid line) and metallic phase (dashed line) for (a) excitation polarized along long axis (b) excitation polarized along short axis. Au Nanocuboid (Length = 180 nm, Width = 30, 60, 90, 120, 150, 180 nm, Height = 40 nm) for VO_2 (10 nm) in semiconducting phase (solid line) and metallic phase (dashed line) for (c) excitation polarized along long axis (d) excitation polarized along short axis.

The VO_2 thin film thickness has a significant effect on the nanoparticle plasmon resonance. Scattering spectra for a Au nanocuboid of length 180 nm, width 90 nm and height 40 nm on VO_2 films with thickness between 10 - 200 nm, are shown in Fig. 3. Different trends can be seen for the semiconducting and metallic phases of VO_2. In the semiconducting phase increasing VO_2 thickness initially strongly redshifts the plasmon peak. For thicker films the dampened peak slowly oscillates between 1300 nm and 1400 nm, attributed to the change in the shape of the VO_2 transmittance spectra between 40–90 nm. For the metallic VO_2 phase, the scattering spectra show a blueshift of the plasmon resonance up to a thickness of 90 nm, after which is only weakly affected by the film thickness. The opposing spectral shifts result in an average $\Delta\lambda$ ($\lambda_{Max[SC]} - \lambda_{Max[M]}$) of 500 nm with a maximum of ~560 nm occurring at 80 nm and 200 nm.

The spectral blueshift seen for all fixed geometries presented in this work, when the underlying VO_2 layer is transitioned from a semiconducting to metallic layer can mainly be attributed to

Optical Materials EXPRESS

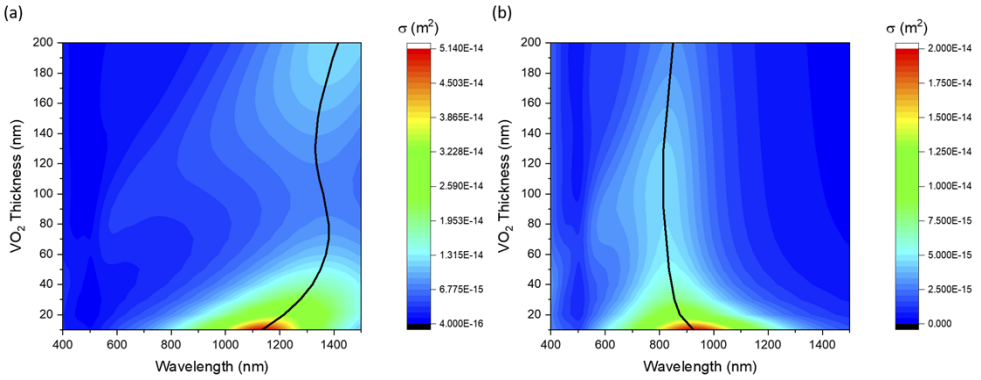

Fig. 3. Contour maps showing the dependence of the scattering cross-section spectrum, for longitudinal excitation, of a Au nanocuboid (Length = 180 nm, Width = 90 nm, Height = 40 nm), on the VO_2 film thickness for VO_2 in (a) semiconducting phase and (b) metallic phase. The scattering peak wavelength is indicated by the black line.

the difference in the real part of the dielectric permittivity. If we consider a simplified case, the polarizability (α) of a small ($r<<\lambda$) Au sphere surrounded by VO_2 can be obtained by solving the Laplace equation. In the case of dipolar excitation, the polarizability can be given as

$$\alpha(\lambda) = r^3 \frac{\tilde{\varepsilon}_{Au}(\lambda) - \tilde{\varepsilon}_{VO_2}(\lambda)}{\tilde{\varepsilon}_{Au}(\lambda) + 2\tilde{\varepsilon}_{VO_2}(\lambda)}$$

The resonance condition occurs when the real part of the denominator vanishes i.e $\tilde{\varepsilon}_{Au}(\lambda) + 2\tilde{\varepsilon}_{VO_2}(\lambda) = 0$ or $\tilde{\varepsilon}_{Au}(\lambda) = -2\tilde{\varepsilon}_{VO_2}(\lambda)$.

The real part of the Au dielectric permittivity is < 0 in the spectral region between 200 -1000 nm and becomes more negative with increasing wavelength. As the real part of the dielectric permittivity of VO_2 decreases from the semiconducting phase to the metallic phase, the resonance condition is satisfied at a shorter wavelength when VO_2 is in its metallic phase. This results in the blueshift of the plasmon resonance peak in metallic phase when compared to semiconducting phase and decrease in peak scattering cross section. Despite the decreased scattering peak, due to the broadness of the resonance feature, a region of increased scattering cross section can be observed. As the shift in wavelength is dependent on the difference in the real part of the dielectric function, a comparison of the values used for the numerical simulations was made to four values from literature [19] and is shown in the SI (Fig. S21.). The change is the real part of the dielectric function used in the simulations presented in this work are comparable to others seen in literature [13] and in some cases more conservative [19].

Figure 4(a) shows comparison of the positions of the longitudinal scattering peak for Au nanorods and nanocuboids with lengths of 180 nm and 230 nm and nanodiscs of diameter 180 nm on a VO_2 thin film of varying thickness. The width and height of the rod and cuboid single nanoparticle structures were fixed at 90 nm and 40 nm, respectively. In the case of the 180 nm long nanoparticles, for VO_2 in semiconducting phase, the resonance peak of the cuboids is the furthest into the infrared. The cuboid resonance peak is between 1135–1415 nm dependent on the underlying VO_2 thickness, the nanodisc response in the semiconducting phase is between 955–1270 nm, a blueshift of up to 295 nm compared to the cuboids. The nanorods demonstrate a further blueshift in the semiconducting scattering peak between 870–1005 nm. This significant redshift for nanoparticles with sharper edges is consistent with previous studies [20]. However, upon the VO_2 phase transition to metallic phase the cuboid scattering peak is significantly less redshifted when compared to the nanodisc and nanorod scattering peak wavelength. The cuboid,

Optical Materials EXPRESS

disc and rod resonance peak wavelengths lie in the ranges 815–925 nm, 755–825 nm and 790–820 nm respectively. Averaging the wavelength shift ($\Delta\lambda$) over all VO_2 thicknesses up to 200 nm results in an average $\Delta\lambda$ of 147.5 nm for the rods, 337.5 nm for the discs and 500.75 nm for the cuboid of similar length. In the case of the larger Au nanorods, an average $\Delta\lambda$ of 317 nm is seen. It is noted that not only is the 230 nm length nanorod plasmon peak significantly blue shifted compared to the 180 nm cuboid for VO_2 in semiconducting phase, in metallic phase the 230 nm nanorod plasmon peak is only 40 nm redshifted when compared to the smaller cuboid. This indicates that the rounding of the plasmonic nanostructure has a significant impact on the magnitude of the wavelength shift when transitioning between the VO_2 phases. This is attributed to the polarization charges being highly localized in the corners of the cuboid structure and therefore having stronger interaction with the VO_2 thin film surface. The resonance feature for the 230 nm long nanocuboid when VO_2 is in semiconducting phase is at 1335 nm for 10 nm VO_2 film thickness and redshifts above 1500 nm, beyond the range of interest in this study. In the metallic phase the resonance feature again lies in the wavelength range between 800–900 nm indicating a plasmon shift of > 600 nm. It is noted that, as for the other nanoparticles, for the semiconducting phase, there is a redshift in peak wavelength with increasingVO_2 thickness, while increasing metallic phase VO_2 thickness blueshifts the scattering spectrum. The full scattering spectra of the Au nanodiscs, nanorods and nanocuboids for both VO_2 phases as a function of VO_2 thickness is given in the supporting information.

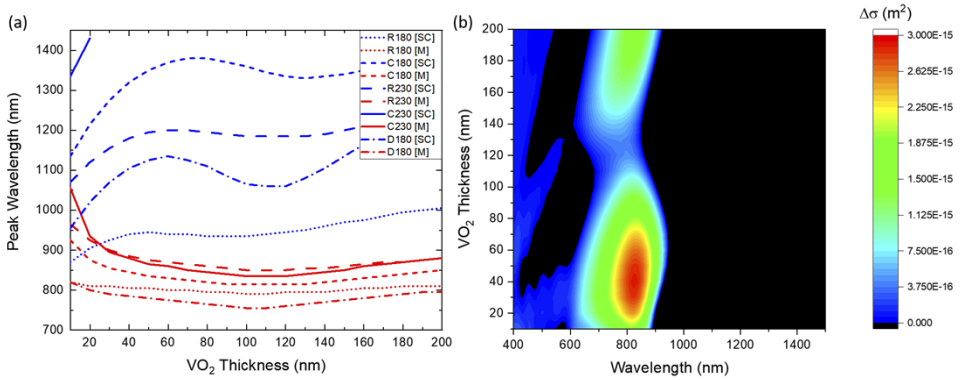

Fig. 4. (a) The dependence of the plasmon resonance peak wavelength on the VO_2 thickness for five Au nanoparticles and VO_2 in semiconducting [SC] and metallic [M] phases under longitudinal excitation; Nanorods of length 180 nm and 230 nm labelled R180 and R230, respectively, nanocuboids of length 180 nm and 230 nm labelled C180 and C230, respectively and nanodiscs of diameter 180 nm labelled D180. The width and height of the nanorods and nanocuboid are fixed at 90 nm and 40 nm (b) Contour map depicting change in scattering cross-section $\Delta\sigma$ ($\sigma_M - \sigma_{SC}$) for Au nanocuboid (Length = 230 nm, Width = 90 nm, Height = 40 nm) with varying VO_2 thickness. Coloured sections indicate an increase in scattering as VO_2 transitions to its metallic phase. Black regions indicate a decrease in scattering as VO_2 transitions to its metallic phase.

Despite the large shift in the plasmon peak wavelength, a decrease in the scattering cross section in the metallic phase results in significant spectral overlap of the scattering spectra for the two phases of VO_2 in the visible and NIR. A contour map of the change in scattering cross section as a function of wavelength and VO_2 film thickness can be seen in Fig. 4(b) for the 230 nm Au nanocuboid. The map indicates the region where the VO_2 phase transition from semiconducting to metallic results in an overall increase in scattering cross section. A maximum $\Delta\sigma$ ($\sigma_M - \sigma_{SC}$) occurs at 830 nm for 40 nm VO_2 thickness. A second region of increased $\Delta\sigma$ occurs for thicker VO_2 and while the plasmonic wavelength shift is larger, increased VO_2 thickness results in a

Optical Materials EXPRESS

lower plasmon cross section due to increased quenching, making thicker film VO_2 less attractive for implementation in plasmonic devices. Additional contour maps (shown in the SI) for nanodisc and nanorod geometries indicate that 30–50 nm VO_2 thin films are optimal for demonstrating an increase in scattering cross section as VO_2 transitions from semiconducting to metallic phase.

We next consider dimer structures consisting of pairs of discs, rods, triangles, and cuboids. Dimer structures are highly advantageous due to the greatly enhanced local electric field in the gap region between the dimer elements. The development of a tunable field enhancement can be employed to provide an enhancement mechanism for coupled quantum emitters [16]. For direct comparison to the single nanoparticle structures considered in the previous section the dimer structures are simulated with similar overall dimensions. A dimer gap of 10 nm is used as this is an experimentally feasible dimer gap that allows the placement of a quantum dot (typical radius 6 nm) [21] within the gap.

Figure 5(a) shows the spectral position of the scattering peak for light polarized along the long axis for a rod dimer (Rod length = 90 nm, Height = 40 nm, Gap = 10 nm), disc dimer (Radius = 45 nm, Height = 40 nm, Gap = 10 nm), cuboid dimer (Length = 90 nm, Height = 40 nm, Gap = 10 nm) and bowtie dimer (Perpendicular bisector = 90 nm, Height = 40nm, Gap = 10 nm). Similar to the single nanoparticles, there is a significant redshift of the plasmon peak for increasing thickness of semiconducting phase VO_2. In the metallic phase, only a nominal 20 nm redshift is observed for all structures. Over the range of VO_2 film thicknesses there is an average peak shift of 35.75 nm, 147.5 nm, 195.25 nm and 202 nm for the rod, disc, cube and bowtie dimer structures, respectively, after the VO_2 phase transition. In Fig. 5(b) the $\Delta\sigma$ contour plot for longitudinal excitation indicates that a maximum percentage increase of 70% in the scattering cross section occurs at 750 nm for a 50 nm thick VO_2 film. This region corresponds to a local maximum in $\Delta\lambda$ (205 nm). As before the bottom lobe in Fig. 5(b) is more favourable due to the reduced damping with a thinner VO_2 film. In the case of the rod dimer the region of increased scattering cross section is blueshifted to 630 nm with a maximum percentage increase of 75% for

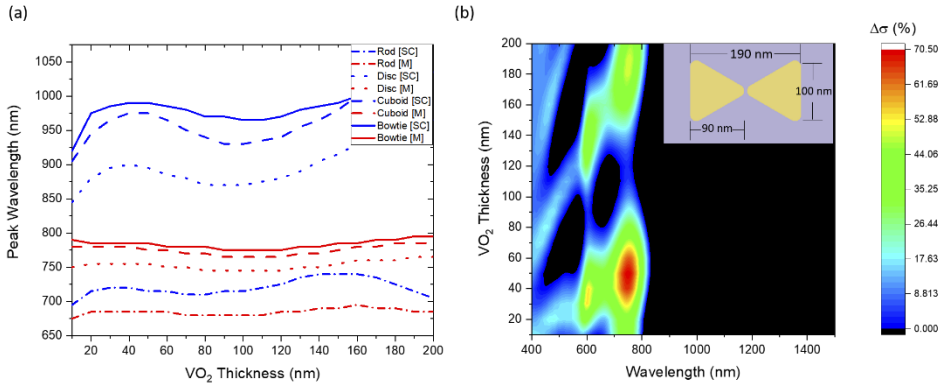

Fig. 5. (a) Dependence of the plasmon resonance peak wavelength on VO_2 thickness for a Au rod dimer (Rod length = 90 nm, Height = 40 nm, Gap = 10 nm), disc dimer (Disc radius = 45 nm, Height = 40 nm, Gap = 10 nm), cuboid dimer (Length = 90 nm, Height = 40 nm, Gap = 10 nm) and bowtie dimer (Perpendicular bisector = 90 nm, Height = 40 nm, Gap = 10 nm) for semiconducting [SC] and metallic [M] phase VO_2 under longitudinal excitation (b) Contour Map depicting $\Delta\sigma$ (%)$[100 \times \frac{(\sigma_M - \sigma_{SC})}{\sigma_{SC}}]$ for Au Bowtie Dimer (Perpendicular Bisector = 90 nm, Height = 40 nm, Gap = 10 nm). Coloured sections indicate an increase in scattering as VO_2 transitions to its metallic phase. Black regions indicate a decrease in scattering as VO_2 transitions to its metallic phase. A schematic of the bowtie dimer structure is included as an inset to (b)

Optical Materials EXPRESS

a 40 nm thick VO_2 film. Plots indicating the regions of increased scattering cross section for disc, cuboid and rod dimers are included in the SI.

An additional advantage of the bowties structure is the enhanced electric field intensity concentrated between the pointed triangles. For investigation of the E-field enhancement

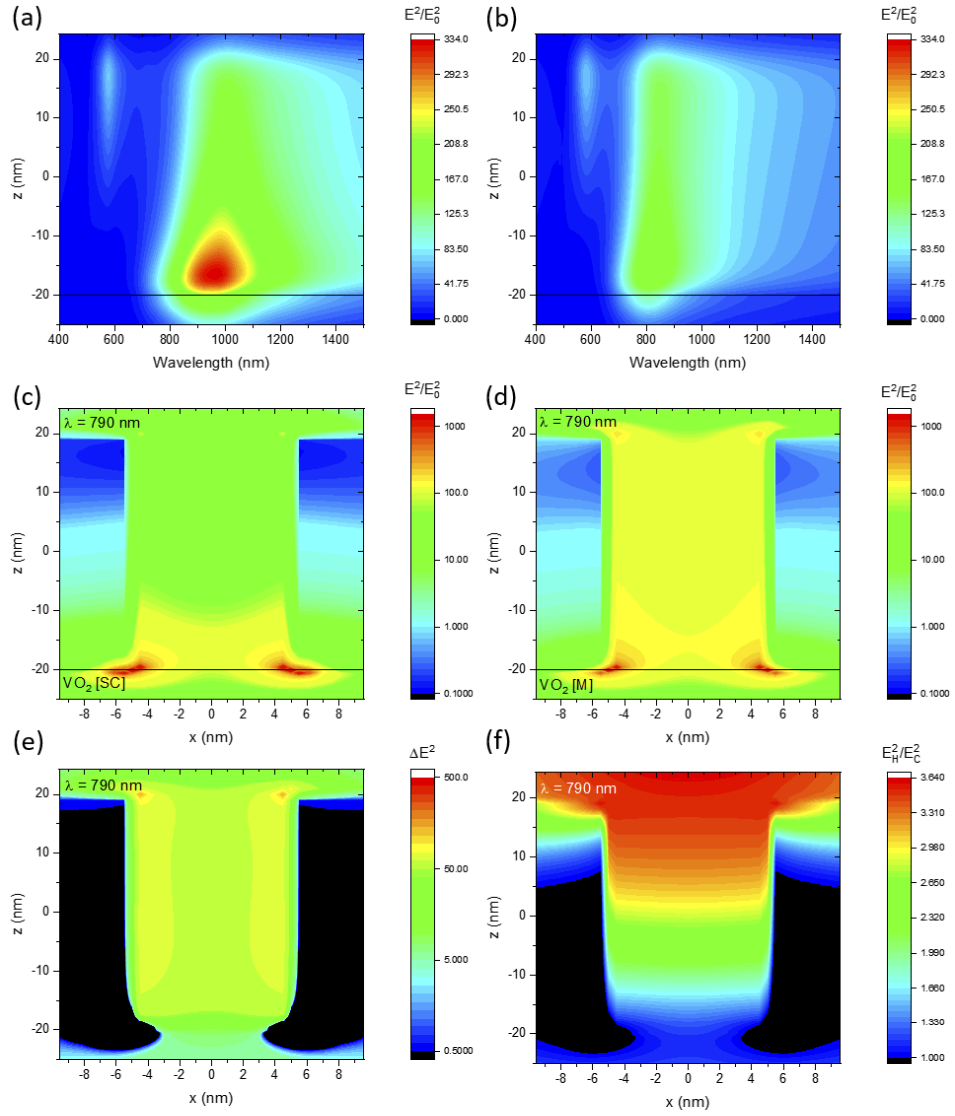

Fig. 6. Contour maps indicating E-field strength between the bowtie elements as a function of dimer height (z) for VO_2 (10 nm) in (a) semiconducting phase and (b) metallic phase. The plane z= -20 nm corresponds to the dimer – VO_2 interface. z = 20 nm indicates the top of the dimer structure. The electric field intensity maps for λ = 790 nm between dimer elements as a function of x-position (along dimer axis) and z-position (along dimer height, perpendicular to VO_2 plane) for VO_2 (10 nm) in (c) semiconducting phase and (d) metallic phase. (e) ΔE^2 ($E_H^2 - E_C^2$) between dimer elements as a function of x-position (along dimer axis) and z-position (along dimer height) for λ = 790 nm and 10 nm VO_2 thickness (f) E_H^2/E_C^2 for λ = 790 nm and 10 nm thickness. All maps are calculated for longitudinal excitation along the dimer axis.

Optical Materials EXPRESS

we consider the Au bowtie dimer structure (Perpendicular bisector = 90 nm, Height = 40 nm, Gap = 10 nm). Figure 6(a) shows the electric field strength in the gap region between the dimer elements as a function of wavelength and z-position for a 10 nm film of both VO_2 phases. The plane z = -20 nm indicates the VO_2 – nanostructure interface and z = 20 nm corresponds to the top of the dimer structure. The VO_2 transition blueshifts the maximum E-field from ~960 nm to ~820 nm, as seen in Fig. 6(b). While the transition results in a decrease in the maximum E-field achieved, at certain wavelengths the E-field is increased. The electric field intensity maps at 790 nm are shown in panels (c) and (d). The VO_2 phase transition effectively increases the strength of the field between the dimer elements and moves the region of enhancement closer to the top surface of the dimer. A positive ΔE^2 ($E_H^2 - E_C^2$) of 90 is observed at $\lambda = 820$ nm and an electric field intensity enhancement of >3.6 is observed at $\lambda = 790$ nm, indicated in Fig. 6(f).

When we consider the same structure on a 30 nm VO_2 film, a redshift in the position of the peak E-field enhancement is observed. This is accompanied with a decrease in peak E-field strength. The reduced E-field intensity in both phases results in a larger E-field enhancement of 7.08. E-field maps for the bowtie dimer structure on 30 nm VO_2 are included in the SI (Fig. S19.).

The E-field enhancement for the cuboid dimer structure (Length = 90 nm, Width = 90 nm, Height = 90 nm, Gap = 90 nm) on VO_2 (10 nm) is similar to the bowtie dimer case ~ 3.6. However, the ΔE^2 value is reduced as the flat edges of the cuboid structure result in a lower enhancement. E-field maps for the cuboid dimer structure are included in the SI (Fig. S20).

3. Conclusion

In this work, we have considered single plasmonic nanoparticles and dimer nanostructures coupled to a thin film of vanadium dioxide to construct widely tunable plasmon resonances. We looked at the factors that affect the magnitude of the plasmon blueshift as the underlying VO_2 film transitions from the low temperature semiconducting phase to high temperature metallic phase, above 68°C. It is found that single cuboid nanoparticles have a significantly larger average $\Delta\lambda$ than rounded nanoparticle shapes of similar dimensions. The average blueshift for a 180 nm long nanocuboid is 501 nm compared to 338 nm for the disc and 148 nm for a nanorod. The resonance for the 230 nm cuboid for VO_2 in semiconducting phase is > 1500 nm and the average peak wavelength in metallic phase is 871 nm indicating that a plasmonic peak shift of well over 630 nm is possible for resonances in the NIR, where the change in dielectric permittivity of VO_2 is larger.

For dimer structures, the cuboid and bowtie dimers demonstrate the largest wavelength shifts of 195 nm and 202 nm, respectively, comparing favorably to the disc and rod dimers which have an average plasmon resonance peak shift of 148 nm and 36 nm, respectively. It is also significant that these sizeable wavelength shifts are accompanied by an increase in the scattering cross-section of 70% at wavelengths r < 900 nm, with Au nanorod dimers demonstrating an increase in scattering cross-section at 630 nm.

Additionally, coupling dimer structures to VO_2 allows for tuning of the enhanced E-field in the dimer gap region. The field maps indicate a change in spatial profile of the E-field intensity with a larger than 3.6-fold increase for the region close to the top of the nanostructure for metallic phase VO_2.

This study has demonstrated that with careful selection the plasmon resonances of nanostructures coupled with a VO_2 thin film can be tuned over a large spectral range. In addition, the scattering cross-section of plasmonic nanostructures can be increased for the metallic phase VO_2. This tunability, coupled with the capacity to thermally, electrically and optically induce the VO_2 phase change, renders hybrid nanoparticle-VO_2 systems a promising candidate for use in optoelectronic systems. These nanostructures can potentially be used in tunable sensing

Optical Materials EXPRESS

arrangements, as building blocks for tunable metasurfaces or for compensation of thermal emission quenching at elevated temperatures.

Funding. Irish Research eLibrary; Science Foundation Ireland (16/IA/4550).

Acknowledgements. We thank Christopher Smith for technical support and the ellipsometry measurements.

Disclosures. The authors declare no conflicts of interest.

Data Availability. Data underlying the results presented in this paper are not publicly available at this time but may be obtained from the authors upon reasonable request.

Supplemental document. See Supplement 1 for supporting content.

References

1. L. Lei, S. Li, H. Huang, K. Tao, and P. Xu, "Ultra-broadband absorber from visible to near-infrared using plasmonic metamaterial," Opt. Express **26**(5), 5686–5693 (2018).
2. T. Chung, S.-Y. Lee, E.-Y. Song, H. Chun, and B. Lee, "Plasmonic nanostructures for nano-scale bio-sensing," Sensors **11**(11), 10907–10929 (2011).
3. A. S. Barker, H. W. Verleur, and H. J. Guggenheim, "Infrared optical properties of vanadium dioxide above and below the transition temperature," Phys. Rev. Lett. **17**(26), 1286–1289 (1966).
4. M. M. Qazilbash, M. Brehm, B.-G. Chae, P.-C. Ho, G. O. Andreev, B.-J. Kim, S.-J. Yun, A. V. Balatsky, M. B. Maple, F. Keilmann, H.-T. Kim, and D. N. Basov, "Mott Transition in VO_2 Revealed by Infrared Spectroscopy and Nano-Imaging," Science **318**(5857), 1750–1753 (2007).
5. B.-G. Chae, H.-T. Kim, D.-H. Youn, and K.-Y. Kang, "Abrupt Metal–Insulator Transition Observed in VO_2 Thin Films Induced by a Switching Voltage Pulse," Phys. B Condens. Matter **369**(1-4), 76–80 (2005).
6. H. W. Verleur, A. S. Barker, and C. N. Berglund, "Optical Properties of VO_2 between 0.25 and 5 EV," Phys. Rev. **172**, 788–798 (1968).
7. A. Zylbersztejn and N. F. Mott, "Metal-insulator transition in vanadium dioxide," Phys. Rev. B **11**(11), 4383–4395 (1975).
8. Y.-C. Her, H. Chen, and Y.-S. Hsu, "Effects of Ag and In Addition on the Optical Properties and Crystallization Kinetics of Eutectic $Sb_{70}Te_{30}$ Phase-Change Recording Film," J. Appl. Phys. **93**(12), 10097–10103 (2003).
9. M. F. Kashif, T. Stomeo, M. A. Vincenti, M. D. Vittorio, M. Scalora, A. D'Orazio, D. de Ceglia, and M. Grande, "Design of vanadium-dioxide-based resonant structures for tunable optical response," Opt. Lett. **47**(9), 2286–2289 (2022).
10. K. Wilson, C. A. Marocico, and A. L. Bradley, "Dynamic structural colour using vanadium dioxide thin films," J. Phys. D: Appl. Phys. **51**(25), 255101 (2018).
11. D. Y. Lei, K. Appavoo, Y. Sonnefraud, R. F. Haglund, and S. A. Maier, "Single-particle plasmon resonance spectroscopy of phase transition in vanadium dioxide," Opt. Lett. **35**(23), 3988–3990 (2010).
12. J. Y. Suh, E. U. Donev, D. W. Ferrara, K. A. Tetz, L. C. Feldman, and R. F. Haglund Jr, "Modulation of the gold particle–plasmon resonance by the metal–semiconductor transition of vanadium dioxide," J. Opt. A: Pure Appl. Opt. **10**(55202), 1 (2008).
13. G. Xu, Y. Chen, M. Tazawa, and P. Jin, "Surface plasmon resonance of silver nanoparticles on vanadium dioxide," J. Phys. Chem. *B* **110**(5), 2051–2056 (2006).
14. G. Xu, C. M. Huang, P. Jin, M. Tazawa, and D. M. Chen, "Nano-Ag on Vanadium Dioxide. I. Localized Spectrum Tailoring," J. Appl. Phys. **104**, 1–7 (2008).
15. G. Xu, C. M. Huang, M. Tazawa, P. Jin, and D. M. Chen, "Nano-Ag on Vanadium Dioxide. II. Thermal Tuning of Surface Plasmon Resonance," J. Appl. Phys. **104**, 1–7 (2008).
16. S. Cunningham, C. Hrelescu, and A. L. Bradley, "Plasmonic nanodiscs on vanadium dioxide thin films for tunable luminescence enhancement," Opt. Express **29**(14), 22288–22298 (2021).
17. P. Kepič, F. Ligmajer, M. Hrtoň, H. Ren, L. d, S. Menezes, S. A. Maier, and T. Šikola, "Optically Tunable Mie Resonance VO_2 Nanoantennas for Metasurfaces in the Visible," ACS Photonics **8**(4), 1048–1057 (2021).
18. L. Lu, Z. Dong, and F. Tijiptoharsono, "Reversible Tunaing of Mie Resonances in the Visible Spectrum," ACS Nano **15**(12), 19722–19732 (2021).
19. C. Wan, Z. Zhang, D. Woolf, C. M. Hessel, J. Rensberg, J. M. Hensley, Y. Xiao, A. Shahsafi, J. Salman, S. Richter, Y. Sun, M. M. Qazilbash, R. Schmidt-Grund, C. Ronning, S. Ramanathan, and M. A. Kats, "On the optical properties of thin-film vanadium dioxide from the visible to the far infrared," Ann. Phys. **531**(10), 1900188 (2019).
20. T.V. Raziman and O.J. Martin, "Polarisation charges and scattering behaviour of realistically rounded plasmonic nanostructures," Opt. Express **21**(18), 21500 (2013).
21. O. Bitton, S. N. Gupta, and G. Haran, "Quantum dot plasmonics: from weak to strong coupling," Nanophotonics **8**(4), 559–575 (2019).